Available online at www.sciencedirect.com

ScienceDirect

Mendeleev Commun., 2024, **34**, 93–96

Mendeleev Communications

Ultrasound irradiation of hydrothermally engineered sub-20 nm PbS nanoparticles and effect of their size on *Aspergillus* species morphology

Ghada Abd-Elmonsef Mahmoud[a] and Ahmed B. M. Ibrahim*[b]

[a] *Department of Botany & Microbiology, Faculty of Science, Assiut University, 71516 Assiut, Egypt. E-mail: ghadamoukabel@aun.edu.eg*

[b] *Department of Chemistry, Faculty of Science, Assiut University, 71516 Assiut, Egypt. E-mail: aibrahim@aun.edu.eg*

DOI: 10.1016/j.mencom.2024.01.028

Lead sulfide nanoparticles were hydrothermally synthesized and their size was diminished *via* exposure to ultrasound waves. Both *h*-PbS and *h,us*-PbS nanoparticles of different sizes were characterized using powder X-ray diffraction, TEM microscopy and surface area measurements. The nanoparticles limited the growth of *Aspergillus* pathogens and light microscopy proved severe morphological abnormalities in the fungal vesicles, conidiophores and mycelia in response to the nanoparticles.

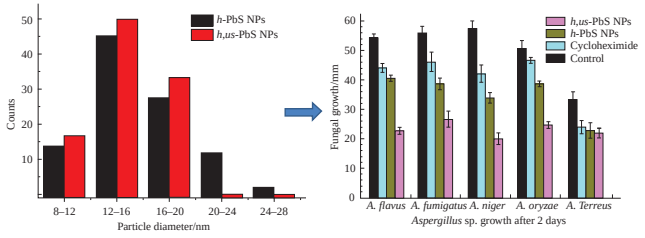

Keywords: nanomaterials, lead sulfide, mesoporous, fungi, morphological abnormalities, pathogens.

Common pathogens *Aspergillus* inhabit numerous air, plant, soil and water habitats.[1] In human, they cause aspergillosis, asthma, allergy and other opportunistic diseases.[1] Indeed, *Aspergillus* can spread fast in windy air causing its conidia to transport particularly to immune-compromised and allergic persons[2] and the airborne fungal conidia, as asexual, can efficiently adapt to many environmental conditions leading to production of more tolerant sexual ascospores.[3] According to literature, *A. flavus*, *A. fumigatus*, *A. niger* and *A. terreus* are the most considerable human and animal pathogenic species[4] and *A. fumigatus* causes ~90% of the human infections.[5]

On the other hand, lead sulfide nanoparticles (PbS NPs) are increasingly synthesized by solvothermal,[6] mechanochemical,[7] phase-transfer,[8] sonochemical,[9] microwavical[10] and even microbial assisted[11] methods for intense utilization in several IR detectors, gas sensors and other applications.[12–15] These nanoparticles, when accumulate in the environment and biological bodies, could bind, disrupt and penetrate the cell membranes, generate intracellular reactive oxygen species and alter the DNA and protein structures resulting in major health problems.[16,17]

This communication reports hydrothermal synthetic procedures of small size PbS NPs from a lead carboxylate compound and thiourea. These precursors for the nanoparticles synthesis were chosen considering their thermal instability that, for the carboxylate complexes, results from the formation of unfavorable four membered chelate rings upon coordination.[18,19] Further, we studied the effect of high power ultrasonication on downsizing the nanoparticles in order to get them optimized for a variety of possible applications. In addition, due to known toxicity of lead compounds, we here selected to study how these nanoparticles affect the morphology of living organisms. Specifically in this paper, we used light microscopy to reveal severe *Aspergillus* species' abnormalities induced by the toxic PbS nanoparticles.

2-(2-Chlorophenylamino)benzoic acid (HL) was prepared from 2-bromobenzoic acid and 2-chloroaniline as reported.[18,20] Deprotonating HL with KOH and refluxing the reaction mixture with lead nitrate resulted in a yellow product that was isolated and characterized as $PbL_2 \cdot H_2O$ by elemental, spectroscopic (FT-IR and ^{1}H NMR) and thermal analysis data. The IR spectral data of this compound gave information regarding its structure. The spectrum cleared bidentate binding mode between Pb^{II} and the carboxylate moieties as revealed by the close proximity between the wavenumbers of the complex ν_{asym}(COO) and ν_{sym}(COO) vibrational bands.[21,22] Additionally, the presence of water in the structure was confirmed due to ν_{water}(OH) transition at 3439 cm^{-1}.[19,23] The ^{1}H NMR spectrum of free HL in DMSO-d_6 exhibited resonances (doublet and triplet) assigned to the aromatic protons in the 6.82–7.95 ppm range and two peaks due to NH and COOH protons at 9.83 and 13.15 ppm, respectively. However, in the complex spectrum, only the peak at 13.15 ppm disappeared evidencing deprotonation of the carboxylic acid group in the product and all other peak positions were almost not changed.

Thermogravimetric analysis (Figure 1) of $PbL_2 \cdot H_2O$ proved clear weight loss of 2.89% up to 150 °C indicating the presence of a hydration water molecule (theoretical 2.51%), and then the residue remained almost resistive to the temperature until ~300 °C. However, this nanoparticle precursor decomposed fast at $T > 300$ °C, and the final decomposition product at 620 °C corresponded to residual PbO (calc. 31.19%; found 30.29%). Other analyses of $PbL_2 \cdot H_2O$ were not accessible due to its practical insolubility even in hot solvents. This prohibited studying its solution characteristics and indeed limited its ability for crystallization from solution for determining its exact structure, but the usage of $PbL_2 \cdot H_2O$ as a precursor for the preparation of different sized PbS NPs was not influenced.

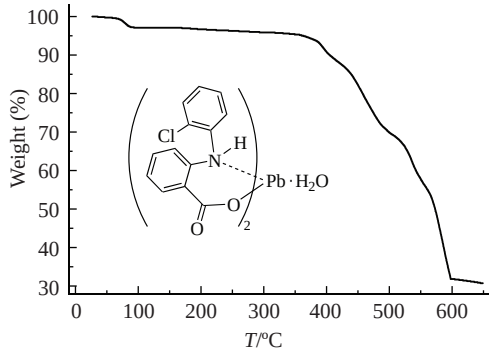

Figure 1 Thermal degradation curve of the nanoparticles precursor.

Carboxylate-metal based compounds that possess unfavorable four-membered rings upon chelation with thiourea, due to their low thermal stability, usually serve for synthesizing metal sulfide nanoparticles.[18,19,24,25] In this work, nanoparticles (*h*-PbS) were synthesized following a hydrothermal route and *h*,*us*-PbS NPs were generated by ultrahigh sonication of the *h*-PbS NPs. As revealed by the nanoparticles' PXRD patterns, *h*-PbS and *h*,*us*-PbS NPs were obtained in high purity, and the exposure of *h*-PbS to ultrasound waves did not change their packing phase. Indeed, the PXRD patterns for *h*-PbS and *h*,*us*-PbS NPs exhibited the same diffraction peaks [(111), (200), (220), (311), (222), (400), (331), (420) and (422)], although the peaks for *h*-PbS were slightly more intense (Figure 2). The diffraction patterns for *h*-PbS and *h*,*us*-PbS NPs showed excellent agreement with the PbS pattern of the ICDD file 04-003-2094 that relates to cubic PbS NPs of the space group *Fm*-3*m*,[26] as all measured diffraction peaks for *h*-PbS and *h*,*us*-PbS are included in this ICDD file.

The nanoparticles' crystallite size was determined by means of Debye–Scherrer equation[24] and transmission electron microscopy (TEM) that both indicated no particles larger than 22 nm in all cases. According to Debye–Scherrer equation, the crystallite size that corresponds to the most predominant PXRD peak (200) is of 22 nm for *h*-PbS NPs and 16 nm for *h*,*us*-PbS NPs. However, TEM (Figure 3) revealed aggregation, irregular morphology and the presence of only a few nanometers' size difference between the particles in both cases since the ultrasound waves diminished the nanoparticles average diameter from 15.9 nm for *h*-PbS NPs to 14.0 nm for *h*,*us*-PbS NPs. Indeed, the disaggregation and improvement in the particles' dispersion and, consequently, the diminishment in the particles' size by high power ultrasonication is a trustworthy reported fast, green, catalyst-free and easy method for size reduction.[27,28] This method based on the development of bubbles and their implosive collapsing in solution leads to cavitation and the development of high pressure and temperature spots during the synthesis.[29]

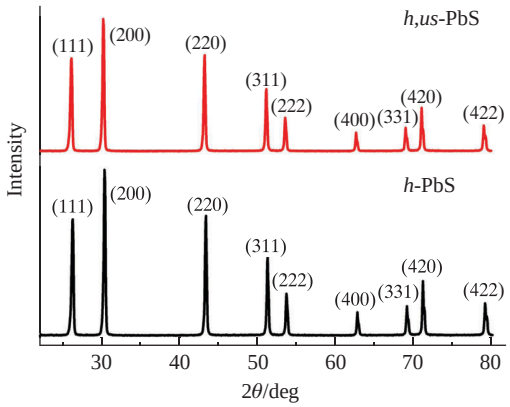

Figure 2 PXRD patterns of *h*-PbS and *h*,*us*-PbS nanoparticles.

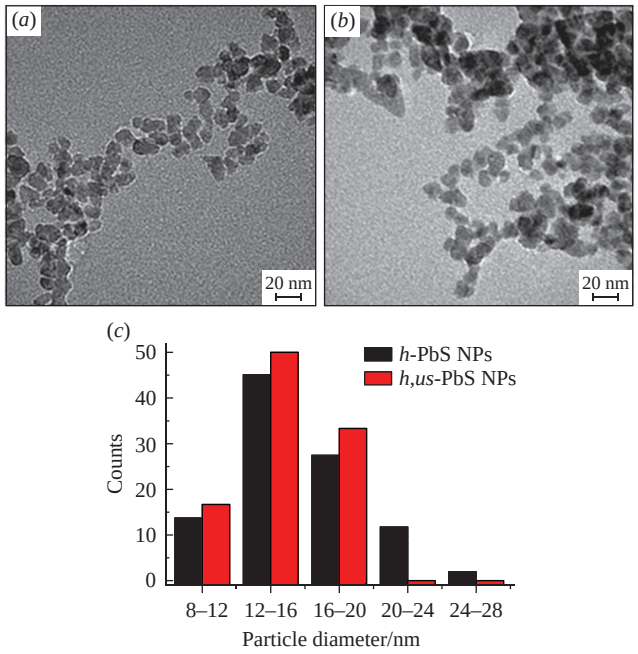

Figure 3 TEM images of (*a*) *h*-PbS and (*b*) *h*,*us*-PbS NPs; (*c*) histogram of nanoparticle size distribution.

Much pronounced differences between *h*-PbS and *h*,*us*-PbS NPs were detected by measuring their nitrogen adsorption/desorption behavior (Table 1). Diminishing the nanoparticles' size by the ultrasound was proved by increasing the nanoparticles' BET surface area from 10.63 $m^2\ g^{-1}$ for *h*-PbS to 15.40 $m^2\ g^{-1}$ for *h*,*us*-PbS. This surface area enhancement was accompanied with an increment in the nanoparticles' average pore diameter from 3.2 to 3.6 nm typical for mesoporous materials in both cases.

The effect of *h*-PbS NPs, *h*,*us*-PbS NPs and cycloheximide on the growth of *A. flavus*, *A. fumigatus*, *A. niger*, *A. oryzae* and *A. terreus* after 2, 4 and 6 days of incubation is shown in Figure 4. Clear results indicated elevated fungal growth inhibition activities of PbS NPs in comparison to inhibition activities displayed by cycloheximide. Besides, elevated fungal growth inhibition by *h*,*us*-PbS NPs in comparison to *h*-PbS NPs was revealed indicating the important role of the PbS NPs' size in fighting the *Aspergillus* microbes. After 2 days of incubation, *A. flavus*, *A. fumigatus*, *A. niger*, *A. oryzae* and *A. terreus* were inhibited by 58.02, 52.40, 65.12, 51.32 and 34.00% by *h*,*us*-PbS NPs, 24.69, 30.95, 40.70, 23.68 and 32.00% by *h*-PbS NPs, and 18.52, 17.86, 26.74, 7.89 and 28.00% by cycloheximide. After 4 days, *A. flavus*, *A. fumigatus*, *A. niger*, *A. oryzae* and *A. terreus* were inhibited by 44.44, 44.79, 58.06, 51.04 and 52.11% by *h*,*us*-PbS NPs, 31.11, 31.25, 30.11, 35.40 and 41.55% by *h*-PbS NPs, and 15.56, 13.54, 16.13, 21.88 and 25.35% by cycloheximide. After 6 days, *A. flavus*, *A. fumigatus*, *A. niger*, *A. oryzae* and *A. terreus* were inhibited by 57.39, 48.28, 50.00, 49.07 and 48.51% by *h*,*us*-PbS NPs, 40.87, 36.20, 27.27, 38.89 and 21.78% by *h*-PbS NPs, and 29.57, 22.41, 20.90, 20.37 and 17.82% by cycloheximide, respectively.

This effectiveness of *h*,*us*-PbS NPs can be attributed to the nanoparticles' smaller size as the smaller the particle size, the

Table 1 Lead sulfide NPs surface areas and porosity parameters.

NP sample	Surface area[a] /$m^2\ g^{-1}$	External surface area[b]/$m^2\ g^{-1}$	Total pore volume /$cm^3\ g^{-1}$	Desorption pore diameter[c]/nm
h-PbS	10.63	9.79	0.017	3.2
h,*us*-PbS	15.40	11.96	0.021	3.6

[a] From BET method. [b] From t-method. [c] From BJH method.

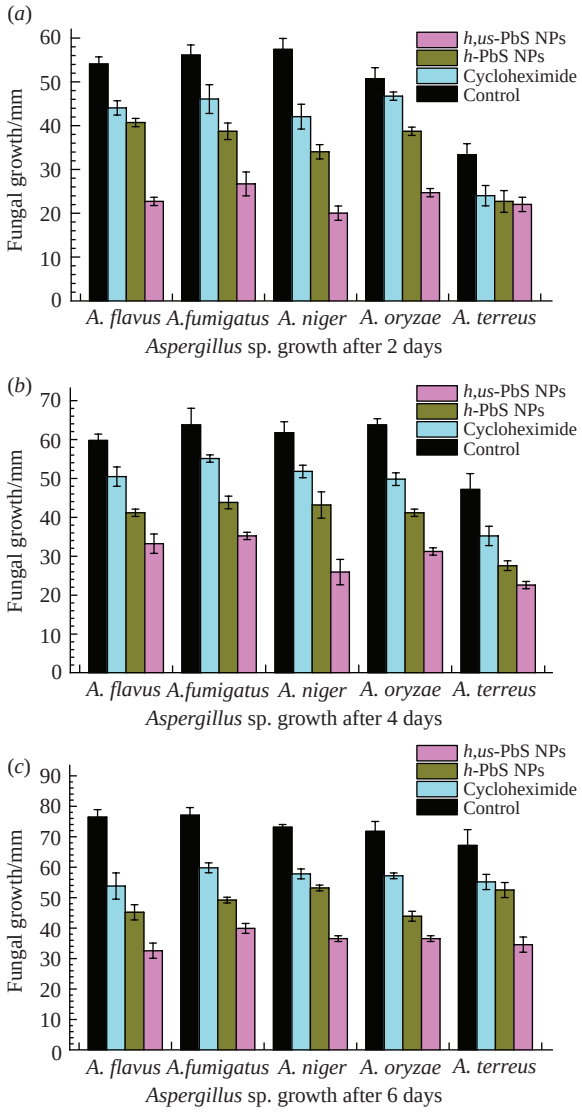

Figure 4 *Aspergillus* growth inhibition by *h*-PbS NPs, *h,us*-PbS NPs and cycloheximide after (*a*) 2 days, (*b*) 4 days and (*c*) 6 days.

higher the ability to bind and transport across the cell membrane. Consequently, the nanoparticles can alter the fungal physiological activities and its growth and can even harm the cellular nuclear components and proteins.[16] In agreement with these results, Kim *et al*. reported that smaller sized silver nanoparticles displayed enhanced inhibition of *E. coli* growth in comparison to larger sized nanoparticles.[30] This is in addition to other reports[31,32] that discussed the relationship between the nanoparticles size of Ag NPs and their antimicrobial activities. This action of the nanoparticles has been commonly attributed to induction of cell oxidative stress that exerts reactive oxygen species which retard the cell anti-oxidation defense system leading to serious mechanical cell membrane damage;[33,34] however, it could also be attributed to release of metal ions[18] or/and other non-oxidative mechanisms.[35] Our findings can also be correlated to the nanoparticles composition as follows: Trivedi *et al*.[36] reported diminishment of *A. flavus* growth by 40% due to the use of lead nanoparticles and Khan *et al*.[37] reported high antifungal activities of lead based nanoparticles with inhibitions reaching 50% against *A. flavus* and *A. niger* and reaching 75% against *C. glabrata*. Moreover, sulfur is known to cause serious effects on both human and animals. According to its antifungal activity, it was used in traditional agriculture to protect vineyards against *Botrytis cinerea*[38] and, in its nanosize, was used for the growth inhibition of *Aspergillus niger*.[39]

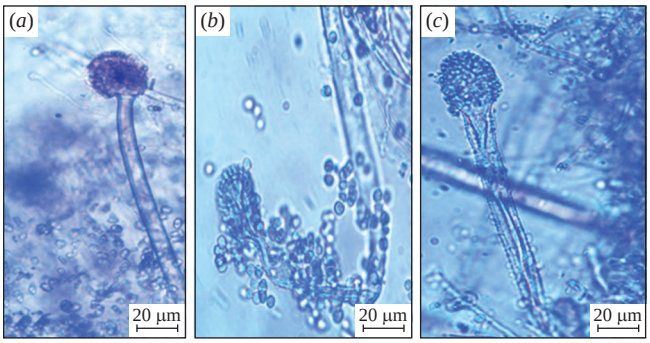

Figure 5 Vesicle deformations in *Aspergillus* species: (*a*) *A. niger*, (*b*) *A. fumigatus* and (*c*) *A. flavus* treated with *h,us*-PbS NPs and *h*-PbS NPs.

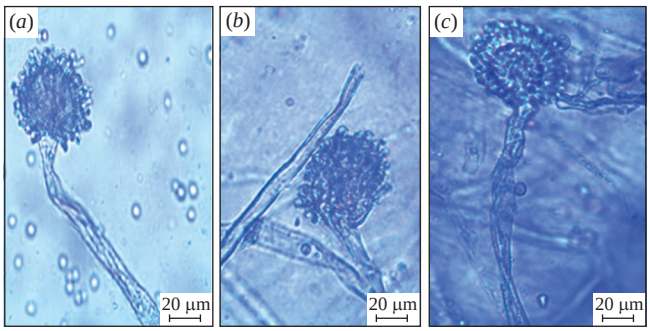

Figure 6 Conidiophores and mycelia deformations in *Aspergillus* species: (*a*) *A. terreus*, (*b*) *A. oryzae* and (*c*) *A. flavus* treated with *h,us*-PbS NPs and *h*-PbS NPs.

Unlike cycloheximide that induced no morphological deformations in comparison with the control samples, PbS NPs caused morphological disturbances. These morphological changes included vesicles deformations (Figure 5) and conidiophores and mycelia deformations (Figure 6). This agrees with previous studies that documented the induction of microbial abnormalities by Pb^{II} compounds: Tian *et al*.[40] reported fungal cell wall enlargement with interlayer distribution and disappearance of normal features of *Aspergillus niger* and *Penicillium oxalicum* cell walls in response to Pb^{II} compounds, while Xu *et al*.[41] discussed the Pb^{II} effect on the reduction of the fungal hypha diameter that led to mycelia elongation and other defects in fungi. Related literature[19] explained morphological deformations regarding the fungal conidia, mycelia and vesicle in the presence of CdS NPs. Therefore, the PbS known high toxicity could be attributed to the observable morphological deformations in the *Aspergillus* species and this effect by the nanoparticles was reported to cause serious mechanical cell membrane damage in fungi resulting in altering their morphology and growth pattern.[16]

To summarize, a lead-carboxylate coordination compound was prepared and served as the lead source for hydrothermal preparation of PbS nanoparticles (average diameter of 15.9 nm and BET of 10.63 $m^2\ g^{-1}$), while ultrasonication of these nanoparticles optimized their characteristics (average diameter of 14.0 nm and BET of 15.40 $m^2\ g^{-1}$) and enhanced their activities. This research provides methods for the synthesis of small size PbS NPs which are nowadays involved in many useful applications. Further, due to known toxicity of PbS nanoparticles, we here emphasized the important role of the nanoparticles size on their toxicity and cleared this toxicity by detecting severe morphological abnormalities in *Aspergillus* species exposed to the nanoparticles.

Financial support of this work from Assiut University (Egypt) is gratefully acknowledged.

Online Supplementary Materials

Supplementary data associated with this article can be found in the online version at doi: 10.1016/j.mencom.2024.01.028.

References

1 H. Ogawa, M. Fujimura, Y. Takeuchi and K. Makimura, *Clin. Exp. Allergy*, 2012, **42**, 1540.
2 M. J. Mendell, A. G. Mirer, K. Cheung, M. Tong and J. Douwes, *Environ. Health Perspect.*, 2011, **119**, 748.
3 T. T. Wyatt, E. A. Golovina, R. Leeuwen, J. E. Hallsworth, H. A. Wösten and J. Dijksterhuis, *Environ. Microbiol.*, 2015, **17**, 383.
4 D. A. Noch, H. A. Ludlam and N. M. Brown, *J. Med. Microbiol*., 2006, **55**, 809.
5 S. A. Balajee, R. Kano, J. W. Baddley, S. A. Moser, K. A. Marr, B. D. Alexander, D. Andes, D. P. Kontoyiannis, G. Perrone, S. Peterson, M. E. Brandt, P. G. Pappas and T. Chiller, *J. Clin. Microbiol.*, 2009, **47**, 3138.
6 Q. Sun, Y. Wang, X. Yuan, J. Han, Q. Ma, F. Li, H. Jin and Z. Liu, *Cryst. Res. Technol.*, 2013, **48**, 627.
7 W. Meng, W. Yuan, Z. Wu, X. Wang, W. Xu, L. Wang, Q. Zhang, C. Zhang, J. Wang and Q. Song, *Powder Technol.*, 2019, **347**, 130.
8 W. Song, C. Wu, H. Yin, X. Liu, P. Sa and J. Hu, *Anal. Lett.*, 2008, **41**, 2844.
9 J. Zhu, S. Liu, O. Palchik, Y. Koltypin and A. Gedanken, *J. Solid State Chem.*, 2000, **153**, 342.
10 M. Salavati-Niasari, A. Sobhani, S. Khoshrooz and N. Mirzanasiri, *J. Cluster Sci.*, 2014, **25**, 937.
11 H.-J. Bai and Z.-M. Zhang, *Mater. Lett.*, 2009, **63**, 764.
12 S. Wang, A. Pan, H. Yin, Y. He, Y. Lei, Z. Xu and B. Zou, *Mater. Lett.*, 2006, **60**, 1242.
13 C. Giansante, I. Infante, E. Fabiano, R. Grisorio, G. P. Suranna and G. Gigli, *J. Am. Chem. Soc.*, 2015, **137**, 1875.
14 Z. L. Wang, X. Y. Kong and J. M. Zuo, *Phys. Rev. Lett.*, 2003, **91**, 185502.
15 D. B. Kuang, A. W. Xu, Y. P. Fang, H. Q. Liu, C. Frommen and D. Fenske, *Adv. Mater.*, 2003, **15**, 1747.
16 L. Wang, C. Hu and L. Shao, *Int. J. Nanomed.*, 2017, **12**, 1227.
17 P.-R. Hsueh, *J. Formosan Med. Assoc.*, 2010, **109**, 685.
18 A. B. M. Ibrahim and G. A.-E. Mahmoud, *J. Inorg. Organomet. Polym. Mater.*, 2019, **29**, 1280.
19 A. B. M. Ibrahim, A. S. A. Zidan, A. A. M. Aly, H. K. Mosbah and G. A.-E. Mahmoud, *Appl. Organomet. Chem.*, 2020, **34**, e5391.
20 A. Sharma and P. Piplani, *Chem. Biol. Drug Des.*, 2017, **90**, 926.
21 D. Kovala-Demertzi, D. Hadjipavlou-Litina, A. Primikiri, M. Staninska, C. Kotoglou and M. A. Demertzis, *Chem. Biodiversity*, 2009, **6**, 948.
22 A. Szorcsik, L. Nagy, J. Sletten, G. Szalontai, E. Kamu, T. Fiore, L. Pellerito and E. Kalman, *J. Organomet. Chem.*, 2004, **689**, 1145.
23 A. Tarushi, C. P. Raptopoulou, V. Psycharis, D. P. Kessissoglou, A. N. Papadopoulos and G. Psomas, *J. Inorg. Biochem.*, 2017, **176**, 100.
24 E. Esmaeili, M. Sabet, M. Salavati-Niasari, Z. Zarghami and S. Bagher, *J. Cluster Sci.*, 2016, **27**, 351.
25 J. D. Patel, F. Mighri, A. Ajji and T. K. Chaudhuri, *J. Nanosci. Nanotechnol.*, 2015, **15**, 2733.
26 Y. Noda, K. Masumoto, S. Ohba, Y. Saito, K. Toriumi, Y. Iwata and I. Shibuya, *Acta Crystallogr.*, 1987, **C43**, 1443.
27 A. B. M. Ibrahim and G. A.-E. Mahmoud, *Appl. Organomet. Chem.*, 2021, **35**, e6086.
28 A. B. M. Ibrahim, G. A.-E. Mahmoud, F. Meurer and M. Bodensteiner, *Appl. Organomet. Chem.*, 2021, **35**, e6134.
29 R. Araya-Hermosilla, J. Martínez, C. Z. Loyola, S. Ramírez, S. Salazar, C. S. Henry, R. Lavín and N. Silva, *Ultrason. Sonochem.*, 2023, **99**, 106545.
30 D. H. Kim, J. C. Park, G. E. Jeon, C. S. Kim and J. H. Seo, *Biotechnol. Bioprocess Eng.*, 2017, **22**, 210.
31 Z. Lu, K. Rong, J. Li, H. Yang and R. Chen, *J. Mater. Sci.: Mater. Med.*, 2013, **24**, 1465.
32 A. Ivask, I. Kurvet, K. Kasemets, I. Blinova, V. Aruoja, S. Suppi, H. Vija, A. Kakinen, T. Titma, M. Heinlaan, M. Visnapuu, D. Koller, V. Kisand and A. Kahru, *PloS ONE*, 2014, **9**, e102108.
33 S. Gurunathan, J. W. Han, A. A. Dayem, V. Eppakayala and J.-H. Kim, *Int. J. Nanomed.*, 2012, **7**, 5901.
34 Y. H. Leung, A. M. C. Ng, X. Xu, Z. Shen, L. A. Gethings, M. T. Wong, C. M. N. Chan, M. Y. Guo, Y. H. Ng, A. B. Djurišić, P. K. H. Lee, W. K. Chan, L. H. Yu, D. L. Phillips, A. P. Y. Ma and F. C. C. Leung, *Small*, 2014, **10**, 1171.
35 A. Nagy, A. Harrison, S. Sabbani, J. R. S. Munson, Jr., P. K. Dutta and W. J. Waldman, *Int. J. Nanomed.*, 2011, **6**, 1833.
36 X. R. Trivedi, T. K. Upadhyay, M. H. Mujahid, F. Khan, P. Pandey, A. B. Sharangi, K. Muzammil, N. Nasir, A. Hassan, N. M. Alabdallah, S. Anwar, S. Siddiqui and M. Saeed, *Processes*, 2022, **10**, 338.
37 Z. U. H. Khan, N. S. Gul, F. Mehmood, S. Sabahat, N. Muhammad, A. Rahim, J. Iqbal, S. Khasim, M. A. Salam, T. M. Khan and J. Wu, *Front. Chem.*, 2023, **11**, 1175114.
38 R. M. Cooper and J. S. Williams, *J. Exp. Bot.*, 2004, **55**, 1947.
39 S. R. Choudhury, M. Ghosh and A. Goswami, *Curr. Microbiol.*, 2012, **65**, 91.
40 D. Tian, Z. Jiang, L. Jiang, M. Su, F. Feng, L. Zhang, S. Wang, Z. Li and S. Hu, *Environ. Microbiol.*, 2019, **21**, 471.
41 X. Xu, R. Hao, H. Xu and A. Lu, *Sci. Rep.*, 2020, **10**, 9079.

Received: 2nd October 2023; Com. 23/7261